PRAMANA
— journal of
physics

Vol. 60, No. 5
May 2003
pp. 921–931

A first look at Au+Au collisions at RHIC energies using the PHOBOS detector

BIRGER BACK[1], for the PHOBOS Collaboration

M D Baker[2], D S Barton[2], R R Betts[6], R Bindel[7], A Budzanowski[3], W Busza[4], A Carroll[2], J Corbo[2], M P Decowski[4], E Garcia[6], N George[1], K Gulbrandsen[4], S Gushue[2], C Halliwell[6], J Hamblen[8], G A Heintzelman[2], C Henderson[4], D Hicks[2], D J Hofman[6], R Hollis[6], R Hołyński[3], B Holzman[2,6], A Iordanova[6], E Johnson[8], J L Kane[4], J Katzy[4,6], N Khan[8], W Kucewicz[6], P Kulinich[4], C M Kuo[5], W T Lin[5], S Manly[8], D McLeod[6], J Michałowski[3], A C Mignerey[7], J Mülmenstädt[4], R Nouicer[6], A Olszewski[2,3], R Pak[2], I C Park[8], H Pernegger[4], M Rafelski[2], M Rbeiz[4], C Reed[4], L P Remsberg[2], M Reuter[6], C Roland[4], G Roland[4], L Rosenberg[4], J Sagerer[6], P Sarin[4], P Sawicki[3], W Skulski[8], S G Steadman[4], P Steinberg[2], G S F Stephans[4], M Stodulski[3], A Sukhanov[2], J-L Tang[5], R Teng[8], A Trzupek[3], C Vale[4], G J van Nieuwenhuizen[4], R Verdier[4], B Wadsworth[4], F L H Wolfs[8], B Wosiek[3], K Woźniak[3], A H Wuosmaa[1] and B Wysłouch[4]

[1]Argonne National Laboratory, Argonne, IL 60439, USA
[2]Brookhaven National Laboratory, Upton, NY 11973, USA
[3]Institute of Nuclear Physics, Kraków, Poland
[4]Massachusetts Institute of Technology, Cambridge, MA 02139, USA
[5]National Central University, Chung-Li, Taiwan
[6]University of Illinois at Chicago, Chicago, IL 60607, USA
[7]University of Maryland, College Park, MD 20742, USA
[8]University of Rochester, Rochester, NY 14627, USA

Abstract. The PHOBOS detector has been used to study Au + Au collisions at $\sqrt{s_{NN}} = 56, 130,$ and 200 GeV. Several global observables have been measured and the results are compared with theoretical models. These observables include the charged-particle multiplicity measured as a function of beam energy, pseudo-rapidity, and centrality of the collision. A unique feature of the PHOBOS detector is its almost complete angular coverage such that these quantities can be studied over a pseudo-rapidity interval of $|\eta| \leq 5.4$. This allows for an almost complete integration of the total charged particle yield, which is found to be about $N_{\rm ch}^{\rm tot} = 4200 \pm 470$ at $\sqrt{s_{NN}} = 130$ GeV and $N_{\rm ch}^{\rm tot} = 5300 \pm 530$ at $\sqrt{s_{NN}} = 200$ GeV.

The ratio of anti-particles to particles emitted in the mid-rapidity region has also been measured using the PHOBOS magnetic spectrometer. Of particular interest is the ratio of anti-protons to protons in the mid-rapidity region, which was found to be $\overline{p}/p = 0.6 \pm 0.04(\text{stat}) \pm 0.06(\text{syst})$ at $\sqrt{s_{NN}} = 130$ GeV. This high value suggests that an almost baryon-free region has been produced in the collisions.

Keywords. Charged particle multiplicity; ultra-relativistic heavy-ion collisions.

PACS No. 25.75.-q

1. Introduction

The early evolution of the universe is believed to have included a short period of extreme energy density allowing for a deconfined state of quarks and gluons (QGP). The re-creation of the QGP in the laboratory may be possible by colliding heavy ions at ultra-relativistic energies to provide an extended volume of extremely high energy density. This goal has been pursued at several accelerators including the Brookhaven AGS and the CERN SPS. Presently the search is concentrated at the relativistic heavy-ion collider (RHIC) at Brookhaven National Laboratory, which is now capable of colliding two Au beams at a center-of-mass energy of up to $\sqrt{s_{NN}} = 200$ GeV. Although no specific signal indicative of the attainment of this new state of matter has been observed as yet, the charged-particle multiplicities observed indicate that the system has evolved through a state of extremely high energy density for which the existence of hadronic matter is inconceivable [1]. The studies of the charged-particle multiplicity in heavy-ion collisions are therefore important because they provide a testbed for further development and refinement of theoretical and phenomenological models.

The PHOBOS detector has been used to measure charged-particle multiplicities for Au + Au collisions at center-of-mass energies of $\sqrt{s_{NN}} = 56$, 130, and 200 GeV. In this work we present measurements of the energy dependence of charged-particle multiplicity at pseudo-rapidity $|\eta| < 1$, as well as the centrality dependence and full distributions for $\sqrt{s_{NN}} = 130$ and 200 GeV.

2. Experimental arrangement

The experimental arrangement used in these measurements is shown schematically in figure 1. The PHOBOS detector consists of three main components: (1) A trigger counter system composed of two sixteen-element scintillator paddle arrays surrounding the beam line and two zero-degree calorimeters positioned at distances of ± 5.21 m and ± 18.5 m from the nominal interaction point, respectively. (2) An array of single layer silicon pad detectors used for charged-particle multiplicity measurements. The central part of this detector consists of sensors arranged as a $\sim$1 m long octagonal barrel which covers the pseudo-rapidity range $-3 < \eta < 3$. It is augmented by three ring counters placed at distances of 1, 2, and 5 m from the interaction point on either side extending the angular coverage to $0.5^\circ < \theta < 179.5^\circ$ corresponding to $-5.4 < \eta < 5.4$. The frame supporting the octagon barrel also contains the double-layer silicon vertex detector. (3) A double-dipole spectrometer consisting of 2 T magnetic field regions in which charged particle tracks traversing up to 14 layers of silicon pad sensors are reconstructed. Particle momentum is obtained from the curvature of the trajectory and particle identification is achieved by measuring energy loss in silicon which is augmented for high momentum particles by a time-of-flight wall behind one of the spectrometer arms. The geometrical acceptance of the detector system, excluding the spectrometer, is illustrated in figure 2. The large and unique acceptance allows for almost complete measurements of the charged-particle multiplicity in heavy-ion collisions. A more detailed description of the PHOBOS detector is given in [2].

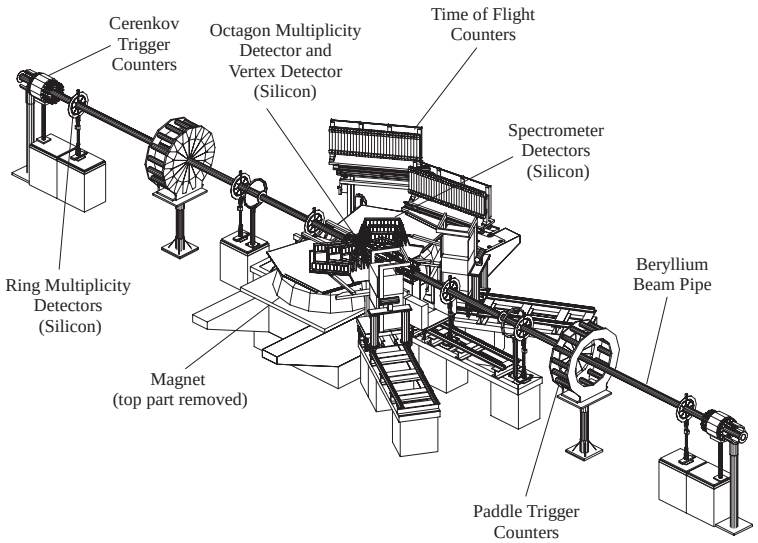

Figure 1. Schematic drawing of the PHOBOS setup. See text for details.

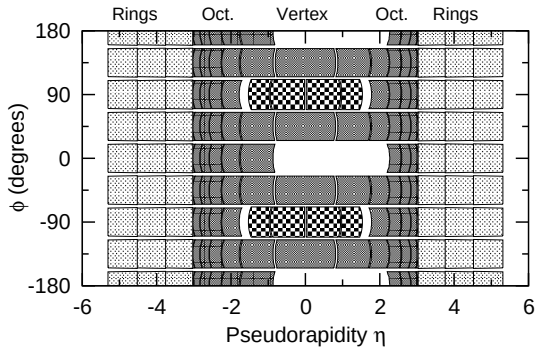

Figure 2. The geometrical acceptances of the ring (light), octagon (medium) and inner vertex (checker board) detectors for particles emitted from the nominal interaction point are shown as a function of η and azimuthal angle ϕ.

3. Triggering and centrality determination

Event triggering is achieved by requiring the coincident detection of ionizing particles in the two paddle counter arrays using the relative timing information to select collisions in a truncated interaction region and reject upstream collisions between the beams and the residual gas molecules in the high vacuum beam-line. Events with a relative time difference of $\Delta t < 4$ ns were accepted. Monte Carlo simulations based on the HIJING event generator [3] show that this trigger configuration responds to about 97% of the total Au + Au inelastic cross-section.

The estimate of the collision centrality was also based on the measured energy deposition in the paddle counters, which has been shown in HIJING simulations to have a monotonic

(almost linear) relationship with the number of participants $N_{\rm part}$ in the collision. The observed cross-section is divided into 18 bins according to the size of the truncated paddle signal (see [4] for further details). Each cross-section bin is related to an average number of participants $\langle N_{\rm part}\rangle$ by comparison with Geant simulations of the Paddle detector response to HIJING events.

4. Charged-particle multiplicities

Measurements of the charged-particle multiplicity at mid-rapidity $|\eta| < 1$ have been obtained by three different types of analysis of PHOBOS data: (1) Simple counting of 'tracklets', i.e., hits in two consecutive Si-detector planes of the vertex or spectrometer detectors in the field-free region close to the vertex position. (2) Counting of hit pads in the single layer octagon detector correcting for multiple hits by assuming Poisson counting statistics. (3) Relating the energy deposition in the single-layer multiplicity counter to the charged-particle multiplicity. Results for all three methods are corrected for non-vertex background and weak-decay feed-down on the basis of Geant/HIJING simulations.

4.1 *Energy dependence at* $\eta = 0$

Charged-particle multiplicity results are shown in figure 3 (solid squares) as a function of the center-of-mass nucleon–nucleon collision energy $\sqrt{s_{NN}}$. In order to compare to $\bar{p}p$ data, the pseudo-rapidity density $\mathrm{d}N/\mathrm{d}\eta$ is divided by the number of binary pairs $\langle \frac{1}{2}N_{\rm part}\rangle$. When compared with results from lower energies (E866/E917 [5] at AGS and NA49 [8] at the CERN SPS) we observe that $\mathrm{d}N/\mathrm{d}\eta/\langle\frac{1}{2}N_{\rm part}\rangle$ for the most central events increases logarithmically with energy up to the recently measured top RHIC energy of $\sqrt{s_{NN}} = 200$ GeV [7] as indicated by the solid line. A comparison to $\bar{p}p$ collisions [9,10] in an overlapping energy region shows a $\sim$55% higher particle production rate in central Au + Au collisions indicating the importance of secondary collisions within the large interaction volume generated in these reactions. However, these data show no sign of any strong enhancement at the top RHIC energy that has been predicted under a jet-quenching scenario within the HIJING model (using default parameters).

This point is illustrated in figure 4, where the measured increase of $14 \pm 5\%$ in $\mathrm{d}N/\mathrm{d}\eta/\langle\frac{1}{2}N_{\rm part}\rangle$ for central Au + Au collisions when the beam energy is increased from 130 GeV to 200 GeV is compared to theoretical predictions as well as the value obtained from an interpolation of $\bar{p}p$ data [10].

4.2 *Centrality dependence at* $\eta = 0$

The centrality dependence of $\mathrm{d}N/\mathrm{d}\eta/\langle\frac{1}{2}N_{\rm part}\rangle$ measured by PHOBOS (solid triangle) at $\sqrt{s_{NN}} = 130$ GeV is compared to similar results obtained by the PHENIX (open triangle) [17] and BRAHMS (open square) [18] experiments in figure 5a. Within the systematic uncertainties indicated by the shaded region there is good agreement between the three experiments and the early PHOBOS measurement [6] (solid square).

In figure 5b the data are compared to predictions of a parton saturation model (EKRT) (dashed–dotted curve) [19] and a decomposition of contributions from soft hadronic and

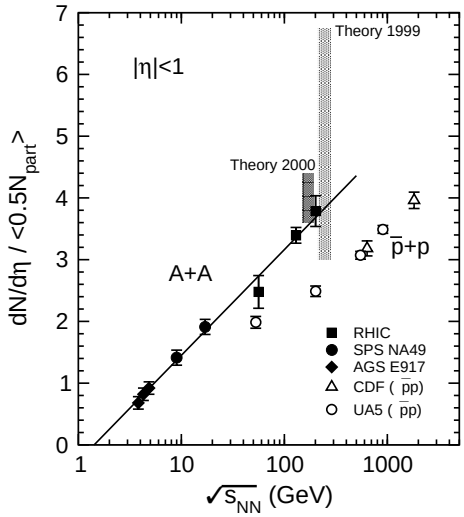

Figure 3. The scaled charged-particle density $\mathrm{d}N/\mathrm{d}\eta/\langle\frac{1}{2}N_{\mathrm{part}}\rangle$ for central Au + Au collisions at AGS [5], RHIC [6,7] and Pb + Pb collisions at the SPS [8] are shown as solid points as a function $\sqrt{s_{NN}}$. The $\bar{p}p$ data from UA5 [9] and CDF [10] are shown as open symbols. The range of theoretical predictions for 200 GeV (light shaded band labeled Theory 1999) [11] are seen to be strongly reduced by the availability of the 130 GeV RHIC data.

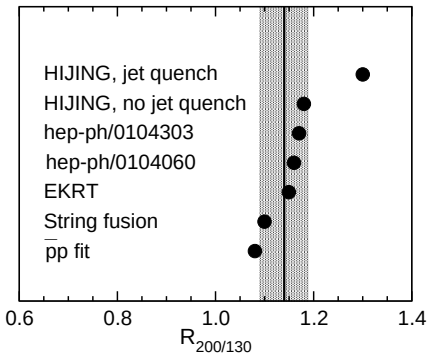

Figure 4. The measured increase in $\mathrm{d}N/\mathrm{d}\eta/\langle\frac{1}{2}N_{\mathrm{part}}\rangle$ with energy from 130 GeV to 200 GeV (shaded band) is compared with theoretical predictions [12–16] and a fit to $\bar{p}p$ data [10]. The shaded band corresponds to the 90% confidence limit.

hard partonic processes proposed by Kharzeev and Nardi [20,21] (dashed curves). The latter is of the form

$$\frac{\mathrm{d}N}{\mathrm{d}\eta} = (1 - x(s))n_{pp}\frac{\langle N_{\mathrm{part}}\rangle}{2} + x(s)n_{pp}\langle N_{\mathrm{coll}}\rangle, \tag{1}$$

where $x(s)$ is the energy dependent contribution of hard collisions N_{coll}. The energy de-

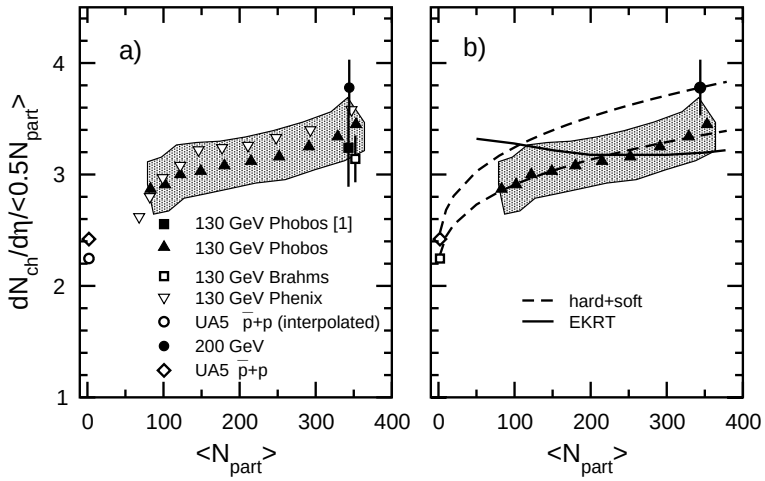

Figure 5. (**a**) Comparison of centrality dependence of $\mathrm{d}N/\mathrm{d}\eta/\langle\frac{1}{2}N_{\mathrm{part}}\rangle$ obtained by PHOBOS (▲), PHENIX (△) and BRAHMS (□) at 130 GeV and PHOBOS at 200 GeV (●). (**b**) Comparison to theoretical predictions (see text).

pendence of $x(s)$ has been derived from inelastic ep scattering data and has been found to scale as $x(s) \propto s^{\lambda}$ with $\lambda \approx 0.25$. The number of hard scattering collisions is found to be $N_{\mathrm{coll}} \approx 0.352(N_{\mathrm{part}})^{1.37}$ [21] and n_{pp} is the experimental value of $\mathrm{d}N/\mathrm{d}\eta$ corresponding to $N_{\mathrm{part}} = 2, N_{\mathrm{coll}} = 1$. Adjusting the value of x to best reproduce the data we find $x(130) = 0.092 \pm 0.018$ and $x(200) = 0.107 \pm 0.018$ which approximately reflect the expected increase based on the $x \propto s^{\lambda}$ scaling.

4.3 *Pseudo-rapidity distributions*

Charged-particle multiplicity distributions for 130 GeV are shown for six centrality bins in figure 6 (see [22] for details). The errors are mostly systematic – the point-to-point statistical errors are substantially smaller. A general feature of these distributions is an almost flat region extending over about two units of pseudo-rapidity around mid-rapidity $\eta = 0$. This region does, however, exhibit a slight minimum at $\eta = 0$, which may be caused by the conversion of a nearly flat rapidity distribution into pseudo-rapidity space. Outside this region we observe a gentle fall-off towards larger $|\eta|$ values. It is also evident that almost the entire distribution falls within the very large η acceptance of the PHOBOS multiplicity detector. This fact allows for a quite accurate estimate of the total charged-particle multiplicity.

A comparison of the multiplicity distributions for central collisions (0–6%) at 130 and 200 GeV is shown in figure 7a. It is evident that additional particle production occurs in the mid-rapidity plateau region and that the width of the distribution is increased at higher energies.

In figure 7b we compare the $\mathrm{d}N/\mathrm{d}\eta$-distribution for $\sqrt{s_{NN}} = 200$ GeV Au + Au with that of $\bar{p}p$ at the same energy [9]. We observe that the increase in charged-particle production in the Au + Au collisions extends over the full η range for which the $\bar{p}p$ data exist although

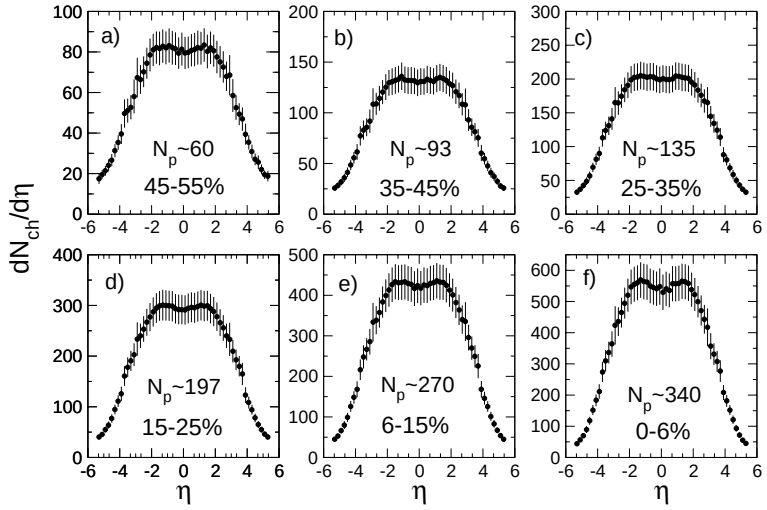

Figure 6. The charged-particle density distributions are shown for six centrality bins denoted by fraction of cross-section and mean number of participants, $\langle N_{\rm part}\rangle$.

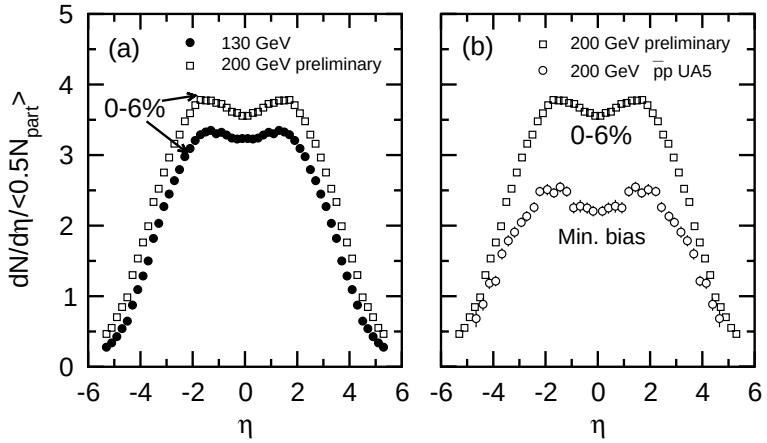

Figure 7. (**a**) Comparison of scaled charged-particle density distributions for 130 GeV (•) and 200 GeV (□) for the 0–6% centrality bin. (**b**) Comparison of the scaled charged-particle density distribution for central Au+Au (□) and $\bar{p}p$ (○) [9] collisions. Systematic errors of 7–10% are not shown for clarity.

the enhancement is slightly stronger in the mid-rapidity region. In $\bar{p}p$ collisions it has been observed that the charged-particle production in the fragmentation region near the beam/target rapidity follows a simple scaling relation as shown in figure 8a. Here, the η distribution of the inelastic cross-section is shown for energies of 53, 200, 546, and 900 GeV [9] as a function of $\eta - y_{\rm beam}$, where $y_{\rm beam}$ is the beam rapidity in the center-of-mass system. In figure 8b we observe that the 130 and 200 GeV $\mathrm{d}N/\mathrm{d}\eta$ distributions for $\mathrm{Au}+\mathrm{Au}$ collisions also follow this limited fragmentation scaling to a remarkable degree down to a value of about $\eta - y_{\rm beam} = -2.5$.

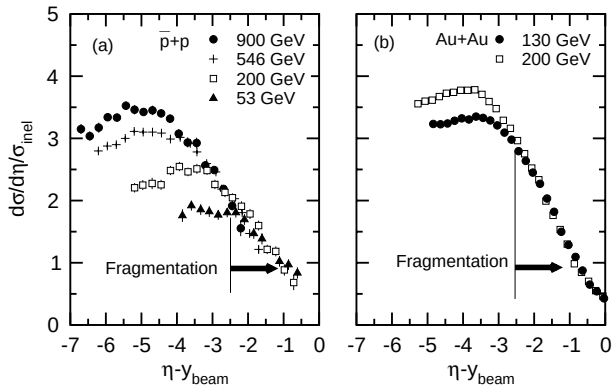

Figure 8. Illustration of scaling in the fragmentation region for $\bar{p}p$ (**a**) and Au + Au (**b**) collisions.

4.4 *Total charged-particle multiplicity*

The total charged-particle multiplicity within the range $-5.4 < \eta < 5.4$ is obtained by integration of the $\mathrm{d}N/\mathrm{d}\eta$ distributions and shown as a function of $\langle N_{\mathrm{part}} \rangle$ in figure 9b for the $\sqrt{s_{NN}} = 130$ GeV data (solid points). For the 200 GeV energy only the most central bin corresponding to 0–6% of the total cross-section is shown (open square). The total particle production scales almost linearly with $\langle N_{\mathrm{part}} \rangle$ and exceeds the prediction of the HIJING model by about 10%. The total charged-particle multiplicity within $-5.4 < \eta < 5.4$ is found to be $N_{\mathrm{ch}}^{\mathrm{tot}} = 4200 \pm 470$ for the 0–3% centrality bin. This value is in good agreement with the value of $N_{\mathrm{ch}}^{\mathrm{tot}} = 3860 \pm 300$ found for the 0–5% centrality bin by the BRAHMS collaboration [18] when integrated over a slightly smaller pseudo-rapidity region of $-4.7 < \eta < 4.7$. At 200 GeV we find $N_{\mathrm{ch}}^{\mathrm{tot}} = 5080 \pm 510$ for the 0–6% centrality bin when integrated over the range $-5.4 < \eta < 5.4$. This corresponds to $N_{\mathrm{ch}}^{\mathrm{tot}} = 5300 \pm 530$ for the 0–3% centrality bin, a ∼25% increase over the 130 GeV value. Also this result is in good agreement with the BRAHMS result of $N_{\mathrm{ch}}^{\mathrm{tot}} = 4639 \pm 370$ [23] for the 0–5% centrality bin in $-4.7 < \eta < 4.7$.

The total charged-particle multiplicity scaled by $\langle N_{\mathrm{part}} \rangle$ is shown in figure 9a as a function of $\langle N_{\mathrm{part}} \rangle$ for both energies (130 GeV: solid points and 200 GeV: open square). The value for the 200 GeV $\bar{p}p$ data [9] extrapolated to the same η range is shown as a solid diamond. We observe only a slight increase in the 130 GeV data over the measured range of $\langle N_{\mathrm{part}} \rangle$. For the 200 GeV data we have performed a fit using the decomposition into 'soft' and 'hard' scatterings (see eq. (1)) resulting in a value of $x = 0.105 \pm 0.020$ for the full $\mathrm{d}N/\mathrm{d}\eta$ distribution (compared with $x = 0.107 \pm 0.018$ for $\mathrm{d}N/\mathrm{d}\eta|_{\eta=0}$).

It is also interesting to examine the widths of the $\mathrm{d}N/\mathrm{d}\eta$ distributions, expressed in terms of the variance (computed over the measured η range). This variance $(var = \sigma^2)$ is observed (figure 9c) to decrease as a function of $\langle N_{\mathrm{part}} \rangle$ for the 130 GeV data (solid circles) reflecting the fact that the increased particle production for more central collisions is concentrated in the mid-rapidity region. Surprisingly, the variance for central Au + Au collisions at 200 GeV (open square) is only slightly smaller than the value obtained in $\bar{p}p$ collisions (solid diamond) [9]. Thus it will be interesting to study the evolution as a function of $\langle N_{\mathrm{part}} \rangle$ for the 200 GeV data once they become available.

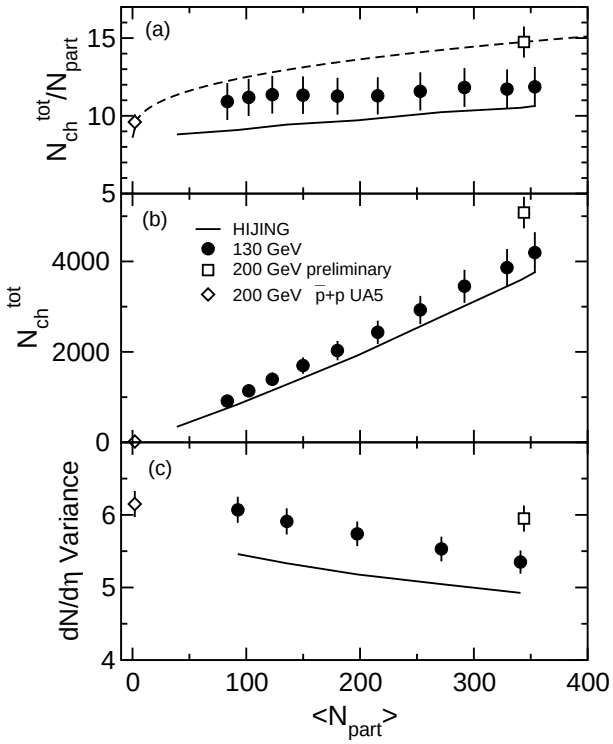

Figure 9. Centrality dependence of (**a**) the total charged-particle multiplicity per average number of participant $\langle N_{\rm part}\rangle$, (**b**) the total charged-particle multiplicity, and (**c**) the variance of the $\mathrm{d}N/\mathrm{d}\eta$ distributions ($-5.4 < \eta < 5.4$) are compared to HIJING calculations (solid curves). See text for details.

5. Anti-particle/particle ratio

It is generally expected that at sufficiently high energies a baryon-free region of high energy density can be formed in central heavy-ion collisions because of insufficient stopping of the incoming baryons. Charged particles emitted in the mid-rapidity region are thus most likely to reflect the degree to which this baryon-free state is attained. It is therefore of interest to measure the ratio of anti-particles to particles in this rapidity region. With PHOBOS this has been done using the magnetic spectrometer with up to 14 Si-detector planes for momentum measurement and particle identification obtained from the curvature of charged particle tracks in the magnetic field regions and the average energy deposition in the Si detectors [24]. Magnetic field reversals allowed for the determination of the ratio of negative to positive particles of the same mass without detailed knowledge of the detection and track-finding efficiencies of the spectrometer since such efficiencies cancel out in the ratio.

The negative-to-positive particle ratio is shown for pions, kaons and protons/anti-protons in figure 10b as a function of particle mass. The data obtained by PHOBOS are represented by solid points while results [27] from the STAR collaboration are shown as open circles.

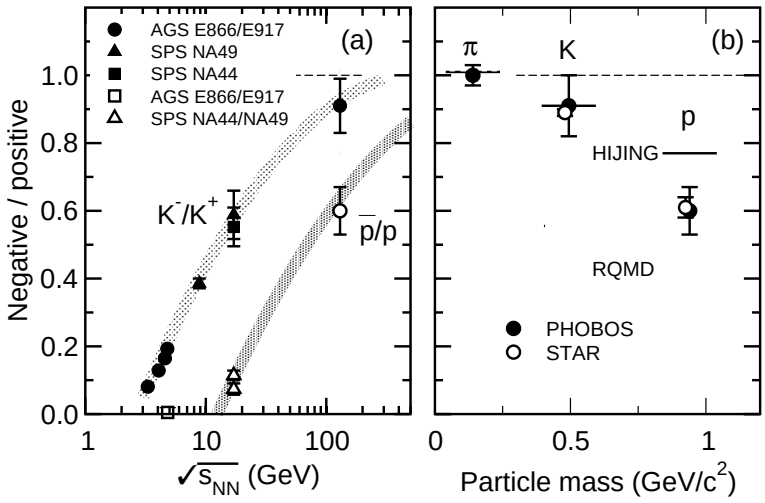

Figure 10. (**a**) K^-/K^+ and $\bar{p}/p$ ratio shown as a function of energy [8,25,26]. The wide bands are drawn to guide the eye. (**b**) π^-/π^+, K^-/K^+ and $\bar{p}/p$ ratios for 130 GeV Au + Au collisions (•, PHOBOS [24]) and (○, STAR [27]), compared to HIJING [16] (—) and RQMD [28] (- - -) predictions.

There is an excellent agreement between the two measurements. It is clear that the baryon-free mid-rapidity region is not yet achieved at $\sqrt{s_{NN}} = 130$ GeV shown here although a substantial increase in the $\bar{p}/p$ ratio is achieved when compared to the SPS data shown in figure 10a as open triangles [8,25]. A thermal model analysis of the anti-particle/particle ratios [29] shows that a baryo-chemical potential of $\mu_B = 45 \pm 5$ MeV and a freeze-out temperature of 160–170 MeV reproduces the observed ratios. This represents a drastic reduction from the value of $\mu_B = 240$–270 MeV found at SPS energies [30].

6. Summary and conclusion

The first results from Au + Au collisions at RHIC energies obtained with the PHOBOS detector have been described. The charged-particle multiplicity has been measured as a function of collision centrality and energy over an extended range of pseudo-rapidity $-5.4 < \eta < 5.4$, which allows for an accurate estimate of the total charged-particle production. For the most central collisions about 4200 charged particles are emitted at 130 GeV reaching about 5300 at the top RHIC energy of $\sqrt{s_{NN}} = 200$ GeV. The energy dependence of charged-particle production at mid-rapidity is shown to follow a logarithmic dependence, which appears to exclude some model predictions including a jet-quenching mechanism. From the measured ratio of anti-protons to protons at mid-rapidity $\langle\bar{p}\rangle/\langle p\rangle = 0.6$ at 130 GeV we derive a baryo-chemical potential of $\mu_B = 45 \pm 5$ MeV for a freeze-out temperature of 160–170 MeV from a thermal model analysis. A large amount of data have already been obtained during the two year operation of the RHIC facility that severely constrain theoretical models for ultra-relativistic heavy-ion collisions.

Acknowledgements

This work was partially supported by (US) DOE grants DE-AC02-98CH10886, DE-FG02-93ER40802, DE-FC02-94ER40818, DE-FG02-94ER40865, DE-FG02-99ER41099 and W-31-109-ENG-38, NSF grants 9603486, 9722606 and 0072204, (Poland) KBN grant 2 P03B 04916, (Taiwan) NSC contract NSC 89-2112-M-008-024.

References

[1] L McLerran, *Pramana – J. Phys.* **60**, 765 (2003)
[2] B B Back *et al*, *Nucl. Instrum. Meth.* A, in press
[3] M Gyulassy and X N Wang, *Comp. Phys. Comm.* **83**, 307 (1994)
[4] B B Back *et al*, *Nucl. Phys.* **A698**, 555 (2002)
[5] L Ahle *et al*, *Phys. Lett.* **B476**, 1 (2000)
L Ahle *et al*, *Phys. Lett.* **B490**, 53 (2000)
B B Back *et al*, *Phys. Rev. Lett.* **86**, 1970 (2001)
[6] B B Back *et al*, *Phys. Rev. Lett.* **85**, 3100 (2000)
[7] B B Back *et al*, *Phys. Rev. Lett.* **88**, 22302 (2002)
[8] J Bächler *et al*, *Nucl. Phys.* **A661**, 45 (1999)
S V Afanasiev *et al*, *Nucl. Phys.* **A698**, 104 (2002)
[9] G J Alner *et al*, *Z. Phys.* **C33**, 1 (1986)
[10] F Abe *et al*, *Phys. Rev.* **D41**, 2330 (1990)
[11] N Armesto and C Pajales, *Int. J. Mod. Phys.* **A15**, 2019 (2000)
[12] N Armesto, C Pajares and D Sousa, hep-ph/0104269
[13] K J Eskola *et al*, hep-ph/0106330
[14] A Accardi, hep-ph/0104060
[15] S Barshay and G Kreyerhoff, hep-ph/0104303
[16] X N Wang and M Gyulassy, *Phys. Rev. Lett.* **86**, 3498 (2001)
[17] K Adcox *et al*, *Phys. Rev. Lett.* **86**, 3500 (2001)
[18] I Bearden *et al*, *Phys. Lett.* **B523**, 227 (2001)
[19] K J Eskola, K Kantaje and K Tuominen, *Phys. Lett.* **B497**, 39 (2001)
K J Eskola, K Kantaje, P V Ruuskanen and K Tuominen, *Nucl. Phys.* **B570**, 379 (2000)
[20] D Kharzeev and M Nardi, *Phys. Lett.* **B507**, 121 (2001)
[21] D Kharzeev and E Levin, *Phys. Lett.* **B523**, 79 (2001)
[22] B B Back *et al*, *Phys. Rev. Lett.* **87**, 102303 (2001)
[23] I Bearden *et al*, nucl-ex/0112001
[24] B B Back *et al*, *Phys. Rev. Lett.* **87**, 102301 (2001)
[25] I G Bearden *et al*, *Phys. Lett.* **B388**, 431 (1996)
[26] L Ahle *et al*, *Phys. Lett.* **B490**, 53 (2000); *Phys. Rev.* **C60**, 064901 (1999); *Phys. Rev. Lett.* **81**, 2650 (1998)
[27] C Adler *et al*, *Phys. Rev. Lett.* **86**, 4778 (2001)
[28] H Sorge, *Phys. Rev.* **C52**, 3291 (1995)
[29] K Redlich, *Nucl. Phys.* **A698**, 94 (2002)
[30] P Braun-Münzinger, I Heppe and J Stachel, *Phys. Lett.* **B465**, 15 (1999)